PUBLISHED BY IOP PUBLISHING FOR SISSA
RECEIVED: *May 5, 2009*
ACCEPTED: *May 26, 2009*
PUBLISHED: *June 18, 2009*

4th INTERNATIONAL CONFERENCE ON IMAGING TECHNOLOGIES IN BIOMEDICAL SCIENCES,
FROM MEDICAL IMAGES TO CLINICAL INFORMATION - BRIDGING THE GAP,
22–28 SEPTEMBER 2007,
MILOS ISLAND, GREECE

Fast iterative reconstructions for animal CT

H.-M. Huang,[a,b] **I.-T. Hsiao**[a,c,1] **and M.-L. Jan**[d]

[a] *Department of Medical Imaging & Radiological Sciences, Chang Gung University, 256 Wenhua 1st road, Kwei-Shan, Taoyuan 333, Taiwan, R.O.C.*
[b] *Department of Biomedical Engineering, Case Western Reserve University, 309 Wickenden Building, 10900 Euclid Avenue, Cleveland, Ohio 44106, U.S.A.*
[c] *Molecular Imaging Center, Chang Gung Memorial Hospital, 5 Fu-Shin Street, Kwei-Shan Taoyuan 333, Taiwan, R.O.C.*
[d] *Physics Division, INER, 1000 Wenhua Rd, Longtan, Taoyuan 32546, Taiwan, R.O.C.*
E-mail: ihsiao@mail.cgu.edu.tw

ABSTRACT: For iterative x-ray computed tomography (CT) reconstruction, the convex algorithm combined with ordered subset (OSC) [1] is a relatively fast algorithm and has shown its potential for low-dose situations. But it needs one forward projection and two backprojections per iteration. Unlike convex algorithm, the gradient algorithm only requires one forward projection and one backprojection per iteration. Here, we applied ordered subsets of projection data to a modified gradient algorithm. In order to further reduce computation time, the new algorithm, the ordered subset gradient (OSG) algorithm, can be adjusted with a step size. We also implemented another OS-type algorithm called OSTR. The OSG algorithm is compared with OSC algorithm and OSTR algorithm using three-dimensional simulated helical cone-beam CT data. The performance is evaluated in terms of log-likelihood, contrast recovery, and bias-variance studies. Results show that images of OSG has compatible visual image quality to those of OSC and OSTR, but in the resolution and bias-variance studies, OSG seems to reach stable values with faster speed. In particular, OSTR has better recovery in a smoother region, but both OSG and OSC have better recovery in the high-frequency regions. Moreover, in terms of log likelihood with respect to computation time, OSG has faster convergence rate than that of OSC and similar to that of OSTR. We conclude that OSG has potential to provide comparable image quality and is more computationally efficient, and thus could be suitable for low-dose, helical cone-beam CT image reconstruction.

KEYWORDS: Image reconstruction in medical imaging; Data processing methods

[1] Corresponding author.

doi:10.1088/1748-0221/4/06/P06017

2009 JINST 4 P06017

Contents

1 Introduction **1**

2 Methods **2**
- 2.1 OSC algorithm 2
- 2.2 OSG algorithm 2
- 2.3 OSTR algorithm 2
- 2.4 Simulation 3
- 2.5 Evaluation of image quality 3

3 Results **4**

4 Discussion/conclusion **6**

2009 JINST 4 P06017

1 Introduction

UNLIKE analytical methods, iterative reconstruction (IR) algorithms for computed tomography (CT) are capable of modeling Poisson data noise, detector response and have more flexibility in different system geometries. In addition, iterative reconstruction methods can reduce sampling artifacts in wide-angle cone-beam CT [8], or limited field-of-view data [9]. In particular, they have been shown to outperform the analytical methods in low-count data. However, iterative reconstruction methods are usually slow and require high computational load. Under the need for a fast iterative reconstruction method for CT, Kamphuis and Beekman [1] extended the original convex algorithm [4, 5] to ordered subsets convex (OSC) algorithm by applying the ordered-subset projection at each sub-iteration. They have shown increased speed and various performance of OSC. We are interested in reconstructing wide-angle helical cone-beam CT data from an animal CT scanner in INER, Taiwan [10]. Although OSC is a relatively fast algorithm, it needs one forward projection and two backward projections per iteration. The extra backprojection in OSC might lead to more computation load. Unlike convex algorithm, the gradient algorithm [2] requires only one forward projection and one backprojection per iteration. Here, in order to reduce computation load as in OSC, we apply ordered subsets of projection data to the gradient algorithm [2] and some modification in the step parameter. The new algorithm is called the ordered subset gradient (OSG) algorithm. Another fast OS type algorithm proposed by Erdogan et al [11] called ordered subset transmission (OSTR) algorithm, also requires only one forward and back-projection per iteration. Here, we studied various step parameters in OSG, and compared the results of OSG with those of OSC and OSTR by using simulated 3D helical cone-beam CT data.

This paper is organized as follows: section 2 describes the equations of OSC, OSG and OSTR algorithms. Section 3 provides the simulation, and discussion on the results and parameter setting. Conclusion is given in section 4.

2 Methods

2.1 OSC algorithm

We define the observed CT projection data and blank scan by y_i and b_i with detector bin $i = 1,\ldots,I$, and the attenuation coefficient by μ_j with voxel $j = 1,\ldots,J$. The expected number of projection data can be represented by $E\{\mathrm{y}\} = be^{-A\mu}$. Here the matrix A denotes the system matrix with element A_{ij} indicating the length of the i-th projection line going through voxel j. The update equation of the OSC algorithm [1] for k-th iteration and (s+1)-th subset in voxel j, can be written as

$$\mu_j^{k,s+1} = \mu_j^{k,s} + \omega^k \left\{ \frac{\mu_j^{k,s}}{\sum\limits_{i\in S_s} A_{ij}[(\sum\limits_j A_{ij}\mu_j^{k,s})\hat{y}_i^{k,s}]} \right\} \left[\sum_{i\in s} A_{ij}(\hat{y}_i^{k,s} - y_i) \right], \tag{2.1}$$

and where

$$\hat{y}_i^{k,s} = b_i \exp\left(-\sum_j A_{ij}\mu_j^{k,s} \right) \tag{2.2}$$

is the estimated CT projection data in detector bin i. The weighting factor or step-size parameter, ω^k, is used to ensure the monotonic increase of the log-likelihood.

2.2 OSG algorithm

In [2], the gradient algorithm updated attenuation coefficients by using all projections. Here, we apply ordered subset methods to gradient algorithm, and updates attenuation coefficients $\mu_j^{k,s+1}$ in voxel j, iteration number k, and subset $s+1$ by

$$\mu_j^{k,s+1} = \mu_j^{k,s} + t \left(\frac{\mu_j^{k,s}}{\sum\limits_{i\in s} A_{ij} y_i} \right) \left[\sum_{i\in S_s} A_{ij}(\bar{y}_i^{k,s} - y_i) \right] \tag{2.3}$$

As shown in [5], the gradient algorithm may not increase log likelihood or maintain non-negativity for step size parameters t= 1. To remain non-negativity and ensure the increase of log likelihood, we tried various t's. One of the step-size parameters t_s we used in our studies is

$$t_s = \max_j \left(\sum_{i\in S_s} A_{ij} y_i \Big/ \sum_i A_{ij} y_i \right). \tag{2.4}$$

The primary differences between eq. (2.1) and eq. (2.3) are the step size parameters and the denominator in the second term. In OSC of eq. (2.1), one can see that the denominator requires one backward projection and needs re-calculation at each update. However, the denominator of preconditioner in OSG of eq. (2.3) is calculated only at the beginning of the update, and remains fixed thereafter. Therefore, with the same iteration number, the computation time of OSG is less than that of OSC. This advantage of OSG will be more significant in 3D cone beam and helical CT.

2.3 OSTR algorithm

The other OS type algorithm with similar form to those of OSC and OSG is the OSTR algorithm [11]. The OSTR algorithm is a simultaneous update algorithm based on separable

2009 JINST 4 P06017

paraboloidal surrogates [11], and has the form:

$$\mu_j^{k,s+1} = \mu_j^{k,s} + \left(\frac{L}{\sum_{i \in s} A_{ij}(A_i y_i)} \right) \left[\sum_{i \in S_s} A_{ij}(\bar{y}_i^{k,s} - y_i) \right] \tag{2.5}$$

where L is the number of subsets, and $A_i = \sum_j A_{ij}$.

2.4 Simulation

We used a 3D Shepp-Logan phantom with image size of 128×128×128, and with voxel size of 0.2 mm. There are 4 ROIs in this phantom, including soft tissue, water background, lung and bone. The linear attenuation coefficient for water at 100 keV was 0.17056 cm^{-1} (μ_{water}). We used 0.40682 cm^{-1} (μ_{bone}) for bone, and $1.1 \times \mu_{water}$ for soft tissue, and 0 for lung. The central slice (64th) of this phantom is shown in figure 1(a). The simulated projection data is generated with 3D helical cone beam geometry with 128 bins x 128 slices, pitch =1, and 120 angles over 360°. For the system matrix, we used a multi-ray system [8] for its computation efficiency and accuracy, and a rotation-based matrix along with symmetric properties of the system matrix for further computer memory reduction. The focal length is 83.2 mm and the distance from focal point to the isocenter is 64 mm. We then generated 30 Poisson noise trials, and the counts in each noise trial are 10k. The simulated data are reconstructed with OSC, OSTR and OSG using 12 subsets and with 5, 10, 20, 30, and 50 iterations.

2.5 Evaluation of image quality

To investigate the performance of three algorithms, we computed the following values. The average contrast for 30 noise trials in a region of interest (ROI) is defined by

$$\text{Contrast} = \frac{1}{M} \sum_{m=1}^{M} \frac{|T - B|}{|T + B|} \tag{2.6}$$

where M is the number of noise trials ($m = 1, 2, \ldots, 30$), T is the average activity in ROI and B is the average activity in background (water). The average standard deviation (STD) for 30 noise trials in ROI is calculated by

$$STD = \sqrt{\frac{1}{N} \sum_{j \in ROI} \left[\frac{1}{M-1} \sum_{m=1}^{M} (\mu^m - \overline{\mu})^2 \right]} \tag{2.7}$$

where N is the number of voxel in ROI, and μ^m indicates the reconstruction images of m-th noise trial and $\overline{\mu}$ represents mean reconstructed image over the M noise trials. The average bias for 30 noise trials in ROI is given by

$$Bias = \sqrt{\frac{1}{N} \sum_{j \in ROI} \left[\frac{1}{M} \sum_{m=1}^{M} \mu^m - \mu \right]^2} \tag{2.8}$$

where μ represents the phantom.

2009 JINST 4 P06017

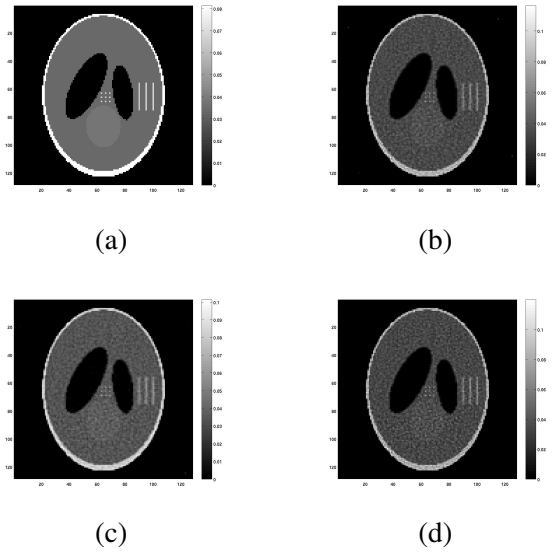

Figure 1. (a) This illustrates the 64-th slice of the 3D phantom with bone, soft tissue, lung and background of water components, and its anecdotal reconstructions of (b) OSC, (c) OSTR, and (d) OSG methods. All reconstructions are with 12 subsets, and 50 iterations.

3 Results

The anecdotal reconstructions of the central slice from OSC, OSTR, and OSG algorithms are displayed in figure 1 (b) (c), and (d) separately, with 12 subsets at 50 iterations. The reconstruction images are visually similar at the same 50 iterations except OSC and OSG seems noisier than OSTR. In addition, OSG looks sharper at the central 9 dots, and the 3 lines in the right hand side of the image. From image profiles not shown here, OSG has better recovery in high frequency components (such as lines and edges) than both OSTR and OSC. This can be illustrated in the line recovery coefficient (RC) plots vs. CPU time in figure 2. Here, RC is defined as reconstructed line intensity divided by the true line intensity. This is more apparent in the early iterations of the reconstruction. This indicates that OSG requires less iteration than OSC and OSTR to reach the same resolution.

From the log-likelihood plot vs. iteration (not shown here), OSC and OSG have similar speed, and faster than OSTR in the beginning. But from the log-likelihood shown as a function of CPU time in figure 3, we can see that the convergent rates of OSG and OSTR are faster than that of OSC. The computation time per iteration for the 3 algorithms are OSC (1.82min) $>$ OSTR (1.25min) = OSG (1.25min). This means that both OSG and OSTR are more efficient than OSC in terms of the log-likelihood value. The advantage will be more significant when image size is getting larger.

The plot of contrast vs. iteration in the soft tissue region is shown in figure 4. The contrast recovery of OSG is slightly better than that of OSC, especially in the early iteration, and both get closer with the increase of iterations. Interestingly, OSTR has higher and almost constant contrast recovery than both OSG and OSC. This is probably due to the smoother result for OSTR as compared to those of OSG and OSC.

In figure 5, we plot bias-STD for soft tissue at 1, 3, 5, 10, 20, 30 and 50 iterations. From this

2009 JINST 4 P06017

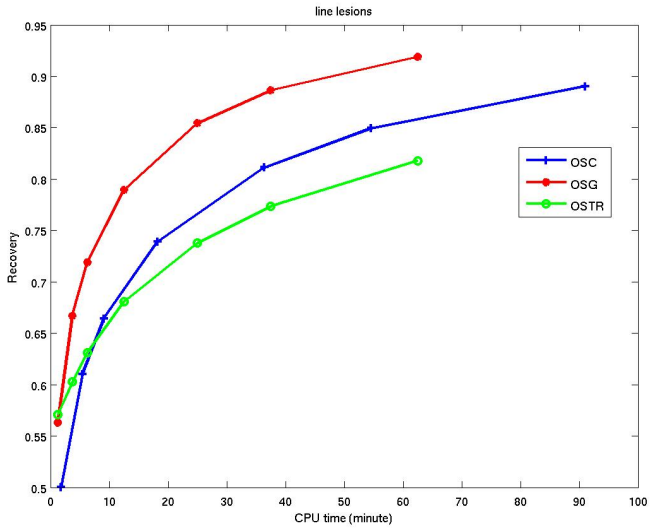

Figure 2. The recovery coefficient (RC) of the line source vs. CPU time is plotted for OSC (+), OSTR (circle) and OSG (dot) reconstructions. Line source RC for OSG converges faster than OSC and OSTR.

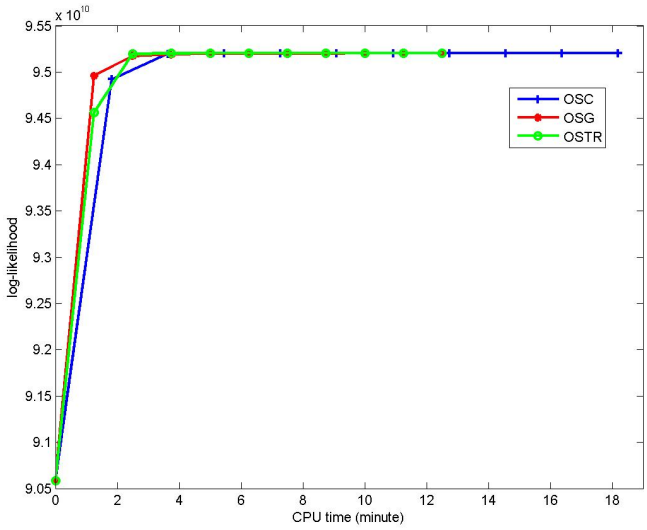

Figure 3. The log-likelihood value vs. CPU time is plotted for OSC (+), OSTR (circle) and OSG (dot) reconstructions. Both OSG and OSTR are faster than OSC in the beginning.

figure, one can see that the bias-STD performances are quite similar for OSC, OSTR and OSG, except that in the first iteration, OSTR has higher bias value. Again, this might come from the fact that OSTR has lower and smoother image in the beginning, and this leads to higher bias values.

2009 JINST 4 P06017

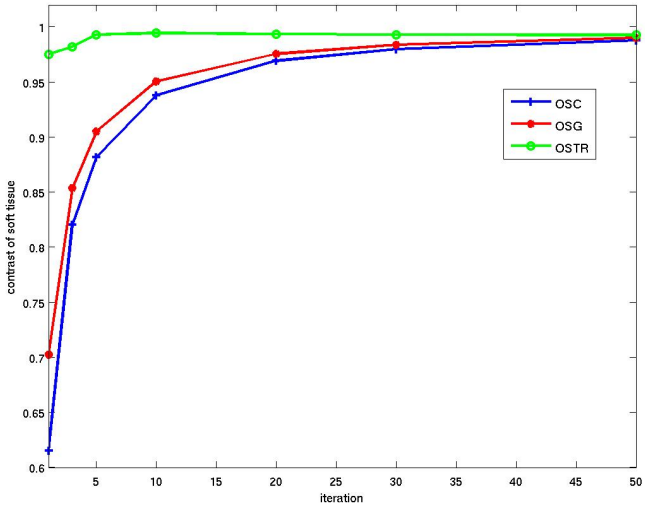

Figure 4. The contrast vs. iteration is plotted for OSC (+), OSTR (circle) and OSG (dot) reconstructions in the soft tissue region. The optimal contrast recovery for the soft tissue should be 1.1.

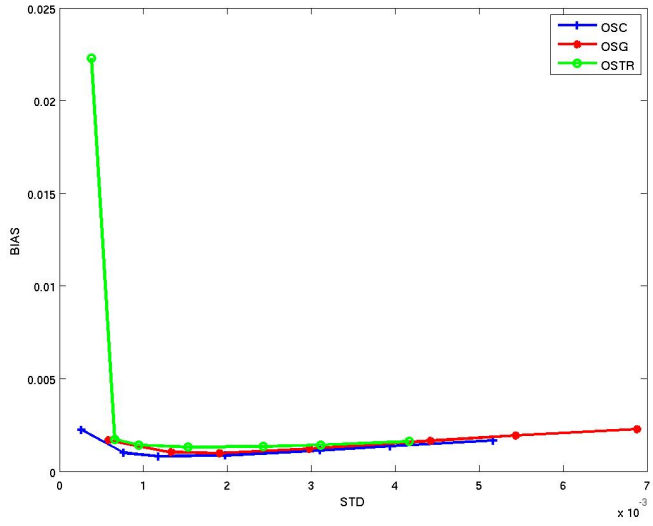

Figure 5. The bias-std curve is plotted for OSC (+), OSTR (circle) and OSG (dot) reconstructions at iteration 1, 3, 5, 10, 20, 30 , and 50. All perform similarly except OSTR has highest bias in the first iteration due to its smooth result.

4 Discussion/conclusion

We have studied an OS version of a modified gradient algorithm for CT reconstruction, and compared its performance to the other two OS algorithms, OSC and OSTR. As compared to OSC, OSG and OSTR need one less backprojection per iteration. In addition, with suitable step parameters, OSG shows faster reconstruction than OSC. The bias-STD studies are similar for all three recon-

structions. We have studied the speeding effect of some step parameters t for OSG. If number of subset L is small, the formula in eq. (2.4) leads to a better performance for OSG than OSC in terms of log-likelihood. However, this speed-up performance does not hold for larger number of subset. We then tried with fixed t, and found out for a fixed t value around 0.6, the performance of OSG shows relatively faster convergence speed than that of OSC, and compatible to that of OSTR independent of subset number L. With this value of 0.6, so far, we have not observed any decrease of log likelihood. However, systematic investigation in t is needed in the future.

From the anecdotal reconstructions, OSC and OSG have noisier result as compared to that of OSTR, and this is consistent with the faster convergence in the high frequency region for OSG (lines and points) while OSTR seems to converge faster in the low frequency region. For future work, we will study the performance of OSG in objects with high variation, and the use of FBP as initial image estimate for further speedup.

In the simulation, we only model the Poisson noise. However, further models on other physical effects including scatter, and system blur, are necessary.

Acknowledgments

This work was supported by a grant INER-962001INER0048 from INER, Taiwan, and by the grant CMRPD34005 from CGMH Research Fund, Taiwan.

References

[1] C. Kamphuis and F.J. Beekman, *Accelerated iterative transmission CT reconstruction using an ordered subsets convex algorithm*, *IEEE T. Med. Imaging* **17** (1998) 1101.

[2] K. Lange, M. Bahn and R. Little, *A theoretical study of some maximum likelihood algorithms for emission and transmission tomography*, *lEEE T. Med. Imaging* **6** (1987) 106.

[3] K. Lange and R. Carson, *E.M. reconstruction algorithms for emission and transmission tomography*, *J. Comput. Assist. Tomo.* **8** (1984) 306.

[4] K. Lange, *An overview of bayesian methods in image reconstruction*, in *Digital image synthesis and inverse optics*, A.F. Gmitro et al. eds., Society of Photo-Optical Engineering, Bellingham U.S.A. (1990).

[5] K. Lange and J.A. Fessler, *Globally convergent algorithms for maximum a posteriori transmission tomography*, *IEEE T. Image Process.* **4** (1995) 1430.

[6] D.S. Lalush et al.i, *Block-iterative techniques for fast* 4*D reconstruction using a priori motion models in gated cardiac SPECT*, *Phys. Med. Biol.* **43** (1998) 875.

[7] R. Siddon, *Fast calculation of the exact radiological path length for a three-dimensional CT array*, *Med. Phys.* **12** (1985) 252.

[8] J. Thibault, K. Sauer, C. Bouman and J. Hsieh, *Three dimensional statistical modeling for image quality improvements in multi-slice helical CT*, in the proceedings of the 8th *International Conference on Fully 3D Reconstruction in Radiology and Nuclear Medicine*, July 6–9, Salt Lake City, U.S.A. (2005).

2009 JINST 4 P06017

[9] C. Michel, F. No, M. Sibomana and D. Faul, *An iterative method for creating attenuation maps from highly truncated CT data*, in the proceedings of the 8th *International Conference on Fully 3D Reconstruction in Radiology and Nuclear Medicine*, July 6–9, Salt Lake City, U.S.A. (2005).

[10] M.-L. Jan et. al., *A combined micro-PET/CT scanner for small animal imaging*, *Nucl. Instrum. Meth.* **A 569** (2006) 314.

[11] H. Erdogan and J.A. Fessler, *Ordered subsets algorithms for transmission tomography*, *Phys. Med. Biol.* **44** (1999) 2835.

2009 JINST 4 P06017